Direct radiative forcing of anthropogenic organic aerosol

Yi Ming

Visiting Scientist Program, University Corporation for Atmospheric Research, Geophysical Fluid Dynamics Laboratory, Princeton, New Jersey, USA

V. Ramaswamy, Paul A. Ginoux, and Larry H. Horowitz

Geophysical Fluid Dynamics Laboratory, Princeton, New Jersey, USA

Received 4 November 2004; revised 12 June 2005; accepted 3 August 2005; published 28 October 2005.

[1] This study simulates the direct radiative forcing of organic aerosol using the GFDL AM2 GCM. The aerosol climatology is provided by the MOZART chemical transport model (CTM). The approach to calculating aerosol optical properties explicitly considers relative humidity–dependent hygroscopic growth by employing a functional group–based thermodynamic model, and makes use of the size distribution derived from AERONET measurements. The preindustrial (PI) and present-day (PD) global burdens of organic carbon are 0.17 and 1.36 Tg OC, respectively. The annual global mean total-sky and clear-sky top-of-the atmosphere (TOA) forcings (PI to PD) are estimated as -0.34 and -0.71 W m^{-2}, respectively. Geographically the radiative cooling largely lies over the source regions, namely part of South America, Central Africa, Europe and South and East Asia. The annual global mean total-sky and clear-sky surface forcings are -0.63 and -0.98 W m^{-2}, respectively. A series of sensitivity analyses shows that the treatments of hygroscopic growth and optical properties of organic aerosol are intertwined in the determination of the global organic aerosol forcing. For example, complete deprivation of water uptake by hydrophilic organic particles reduces the standard (total-sky) and clear-sky TOA forcing estimates by 18% and 20%, respectively, while the uptake by a highly soluble organic compound (malonic acid) enhances them by 18% and 32%, respectively. Treating particles as non-absorbing enhances aerosol reflection and increases the total-sky and clear-sky TOA forcing by 47% and 18%, respectively, while neglecting the scattering brought about by the water associated with particles reduces them by 24% and 7%, respectively.

Citation: Ming, Y., V. Ramaswamy, P. A. Ginoux, and L. H. Horowitz (2005), Direct radiative forcing of anthropogenic organic aerosol, *J. Geophys. Res.*, *110*, D20208, doi:10.1029/2004JD005573.

1. Introduction

[2] Organic species account for a significant fraction of total atmospheric particulate mass [*Duce et al.*, 1983; *Middlebrook et al.*, 1998]. An array of natural and anthropogenic sources are responsible for the production of organic aerosol, which is classified as primary (POA) or secondary organic aerosol (SOA) depending on whether they are emitted as such or are formed from gas precursors in the atmosphere. The burning of fossil fuels and biomass is the main source of POA. Photochemical reactions are able to oxidize volatile gas-phase organic compounds into low vapor-pressure ones, which then either nucleate into new particles or, more likely, condense onto pre-existing particles, thus giving rise to SOA.

[3] Aerosols are capable of affecting the Earth's radiation balance directly through scattering and/or absorbing incoming sunlight in cloudless conditions. Numerous studies were devoted to the computation of direct radiative forcing (DRF) of sulfate aerosol [e.g., *Haywood and Ramaswamy*, 1998; *Adams et al.*, 2001]. In contrast, relatively few exist for organic aerosol [e.g., *Cooke et al.*, 1999; *Koch*, 2001; *Chung and Seinfeld*, 2002; *Liao et al.*, 2004; *Reddy et al.*, 2005]. Although the ways in which organic and sulfate aerosols interact with radiation bear no fundamental difference, they vary in chemical composition, size distribution and other properties relevant for forcing calculation (e.g., solubility and refractive indices). For example, sulfate aerosol is non-absorbing in visible wavelength, while organic aerosol is usually considered as mildly absorbing [*Kanakidou et al.*, 2005]. The estimated DRF of organic aerosol is subject to large uncertainties, which range from -0.04 to -0.41 W m^{-2} for fossil fuel and biomass burning organic carbon (OC) [*Ramaswamy et al.*, 2001]. The need to better understand the radiative effects of organic aerosol necessitates further studies of the treatment of organic aerosol in general circulation models (GCMs).

[4] This paper describes an effort to improve the representation of organic aerosol in a GCM on the basis of some latest experimental and modeling studies. The geographical distributions and seasonal variations of simulated DRF are

0148-0227/05/2004JD005573$09.00

Table 1. Properties of Organic Aerosol Used in Calculating Optical Properties

	OM/OC Ratio	Density, kg m^{-3}
Hydrophilic	1.3	1.0×10^3
Hydrophobic	1.7	1.5×10^3

presented. Sensitivity analyses reveal to what extents hygroscopic growth and optical properties of organic aerosol affect the results.

2. Methodology

[5] The global-scale meteorology and radiative transfer under the impact of organic aerosol are simulated using a modified version of the Geophysical Fluid Dynamics Laboratory (GFDL) AM2 GCM. For a comprehensive review of the model structure and validation, readers are referred to *GFDL Global Atmospheric Model Development Team* [2004]. The GCM resolution for this study is 2.5° in longitude × 2° in latitude, with 24 vertical layers mostly located in the troposphere.

[6] The task of simulating the chemical transport of organic aerosol is handled off-line by the Model for OZone And Related chemical Tracers (MOZART) [*Tie et al.*, 2001; *Horowitz et al.*, 2003; *Tie et al.*, 2005], which considers a variety of gas-phase and heterogeneous chemical reactions, and is driven with the meteorological fields (e.g., winds, temperature, specific humidity and surface pressure) derived from the National Center for Atmospheric Research (NCAR) Community Climate Model (MACCM3). Dry deposition and wet scavenging are the main mechanisms of aerosol removal. The fossil fuel emissions are based on *Cooke et al.* [1999], and the biomass burning emissions are computed from the emission factors of *Andreae and Merlet* [2001] and burning inventories of *Hao and Liu* [1994] and *Mueller* [1992]. The preindustrial (PI) and present-day (PD) OC emissions are 3.8 and 52.3 Tg OC yr^{-1}, respectively. MOZART tracks hydrophobic and hydrophilic OC separately, between which the emissions are equally divided. As a result of atmospheric aging, the conversion from hydrophobic OC to hydrophilic OC has a characteristic timescale of 1.6 days. The monthly mean aerosol climatology from MOZART is read and interpolated by the GCM to provide the time-resolved spatial distribution of organic aerosol.

[7] MOZART simulates the evolution of OC, as opposed to organic mass (OM). The ratio of OM to OC (OM/OC ratio) is necessary for converting the mass of OC to OM. A review by *Turpin and Lim* [2001] concluded that the widely used OM/OC ratio of 1.4 is the lowest reasonable estimate for urban aerosol, and does not represent aged non-urban aerosol well. They recommended 1.6 and 2.1 for urban and non-urban aerosols, respectively, based on measured molecular-level compositions. *Russell* [2003] reported the development of a Fourier Transform-Infrared (FTIR)-based experimental technique that helped reduce the uncertainties in measuring the ratio, and found that over 90% of the samples collected in Asia and the Caribbean have ratios ranging from 1.2 to 1.6. *Liousse et al.* [1996] applied a globally uniform OM/OC ratio of 1.3, which is at the low end of suggested values, to convert simulated OM to OC for comparison with measurements. The same ratio was also used by *Chung and Seinfeld* [2002]. Using 1.3 for hydrophobic OC and 1.7 for hydrophilic OC, this study allows OM/OC ratio to vary with the aging process on the global scale (Table 1). The respective densities are assumed to be 1.0 and 1.5×10^3 kg m^{-3} based on the measured/predicted ranges for different types of organic compounds presented in *Turpin and Lim* [2001] (Table 1). They differ from 1.8×10^3 kg m^{-3}, which has been used in some studies [e.g., *Cooke et al.*, 1999; *Chung and Seinfeld*, 2002; *Reddy et al.*, 2005], but is somewhat high for most organic compounds.

[8] Previous studies of DRF of organic aerosol usually employed assumed size distributions, which vary considerably from study to study. For example, *Reddy et al.* [2005] assumed that OC shares the same lognormal size distribution as sulfate with an effective diameter of 0.24 μm, while *Koch* [2001] and *Chung and Seinfeld* [2002] used the standard gamma distribution with an effective diameter of 1.0 μm according to the Global Aerosol Data Set (GADS) [*Köpek et al.*, 1997]. The AERONET measurements of aerosol optical depth over biomass burning sites of Amazonian forest were utilized to estimate aerosol sizes [*Dubovik et al.*, 2002]. The derived size distribution is composed of two log-normal modes: an accumulation mode and a coarse mode. The number-based mean diameters and standard deviations are 0.185 μm and 1.492, and 1.138 μm and 2.203, respectively. The number concentration ratio of the accumulation mode to the coarse mode is 4.5×10^3. Although other aerosols such as black carbon (BC) and sulfate coexist with organic aerosol over biomass burning regions, organic aerosol is presumed to be the dominant aerosol species owing to much higher emission factor than BC [*Liousse et al.*, 1996] and less significant fossil fuel burning (the main source of sulfate) than biomass burning. The AERONET measurements from which the size distribution was derived were taken during the dry seasons of Amazonian forest, when the average relative humidity (RH) is below 45% according to the National Centers for Environmental Prediction (NCEP) reanalysis data. Organic aerosol remains dry under these conditions. Thus the derived normalized size distribution is deemed as representative of dry organic aerosol, and used in this study to better constrain the forcing determination.

[9] It is well known from experimental evidences gathered both in laboratory and in field that organic particles are able to take up water from ambient humid air, and grow larger in size, a process called "hygroscopic growth". The absorbed water adds to aerosol mass available for scattering sunlight, thus strengthening DRF. *Haywood and Ramaswamy* [1998] and *Adams et al.* [2001] suggested that DRF of sulfate aerosol is very sensitivity to hygroscopic growth; different approaches to calculating the growth lead to a variation of 60%.

[10] One of the aspects in which organic aerosol differs from inorganic aerosol (e.g., sulfate and sea-salt) is chemical composition. While the few inorganic salts (e.g., $(NH_4)_2SO_4$ and NaCl) almost entirely account for inorganic aerosol mass, organic aerosol usually contains a variety of compounds of different structures and properties, posing a challenge for the effort to model the complex mixture in a rigorous way. *Ming and Russell* [2002] proposed a thermodynamic model to predict the equilibrium of aqueous solutions of organic solutes with a limited number of

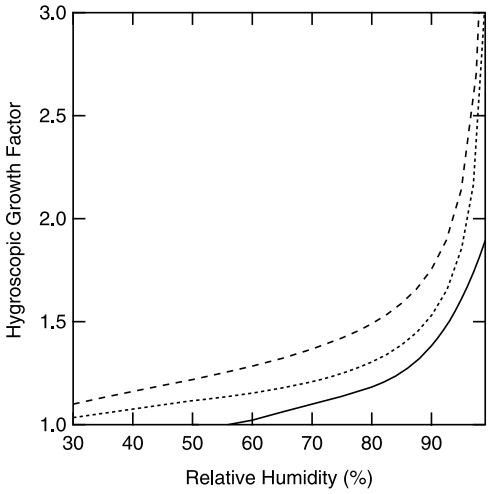

Figure 1. Hygroscopic growth factors of model composition (solid line), malonic acid (dotted line), and ammonium sulfate (dashed line).

interaction parameters between functional groups. The model was employed to calculate the hygroscopic growth factors, defined as ratio of the particle diameter at a specific RH to dry diameter, of laboratory–generated aerosols. The results were in good agreement with laboratory measurements [*Prenni et al.*, 2001]. The parameters are fitted from experimental data at warm temperatures (around 20°C), and the applicability at lower temperatures cannot be reliably assessed due to the lack of experiments. However, high RH and strong impact of hygroscopicity on radiative forcing occur mainly in the boundary layer and lower troposphere, where the temperature is relatively warm.

[11] Only a small fraction of organic aerosol mass was resolved experimentally at the molecular level [*Rogge et al.*, 1993]. In order to bridge the gap between the need for complete chemical composition for modeling purpose and what can be obtained through instrumental analysis, *Ming and Russell* [2001] used four soluble compounds, which are among the most abundant organic species observed in sea water, to represent the soluble organic fraction of sea-salt aerosol. The resulting composition is 60% (by mass) malic acid, 28% citric acid, 6% glucose and 6% fructose. As predicted by the thermodynamic model of *Ming and Russell* [2002], the hygroscopic growth factors based on the model composition were consistent with the field measurements of sea-salt and the so-called ''less hygroscopic'' aerosols [*Ming and Russell*, 2001]. The hygroscopic growth curve is plotted in Figure 1. In this study, the hygroscopicity of hydrophilic OC is based on the same composition and thermodynamic model, while hydrophobic OC is treated as non-hygroscopic. Despite the fact that this composition is originally derived for marine aerosol, the predicted hygroscopic growth is consistent with available measurements of continental aerosol. The Interagency Monitoring of Protected Visual Environments (IMPROVE) study showed that the hygroscopic growth factors of organic aerosol range from 1.1 to 1.2 at 85% over numerous sites located in the continental United States (W. C. Malm et al., Hygroscopic properties of an organic-laden aerosol, submitted to *Atmospheric Environment*, 2005), consistent with the model predictions. *Randles et al.* [2004] showed that the measured increases in scattering by anthropogenically influenced/polluted aerosols due to hygroscopic growth agree well with the model predictions for water soluble organic compounds (WSOC). One possible explanation for the similarity in hygroscopicity between marine and continental organic aerosols is that hygroscopicity is determined mainly by the polarity of component compounds, instead of specific chemical structures, and both organic aerosols may have comparable polarity. The RH fields used in calculating hygroscopic growth factors are supplied by the GCM.

[12] Due to the lack of measurements of the refractive indices of organic aerosol [*Kanakidou et al.*, 2005], they are assumed to be the same as those of the ''water-soluble'' aerosol of GADS [*Köpek et al.*, 1997], whose real and imaginary parts in visible wavelength are 1.53 and 0.006, respectively. Previous studies like *Cooke et al.* [1999], *Chung and Seinfeld* [2002], and *Reddy et al.* [2005] made the same assumption. These values are used in the standard model calculations below. The imaginary part is much higher than that of ammonium sulfate (1×10^{-7}). Consequently, organic aerosol is treated as mildly absorbing in this study. The refractive indices of wet particles are calculated from those of dry organic aerosol and water using the volume averaging rule.

[13] This study assumes that organic aerosol is externally mixed with other aerosol types. As calculated from the OM/OC ratios, densities, normalized size distribution, hygroscopic growth factors and refractive indices based on the Mie theory, the optical properties, namely OC mass–based extinction coefficient (σ_e), single-scattering albedo (ω) and asymmetry factor (g), at 40 different wavelengths are computed for hydrophobic and hydrophilic OC for the purpose of calculating layer reflection and transmission using the δ-Eddington technique. The results in visible wavelength are listed as BASE in Tables 2a and 2b, respectively. Besides organic aerosol, the GCM also takes into account the radiative effects of sulfate, sea-salt, BC and dust aerosols, which remain fixed in the simulations reported here.

[14] DRF is estimated using the average flux change resulting from instantaneously switching to PD concentrations from PI at every radiation time step (3 hours) on the 15th day of each month. *Haywood et al.* [1998] employed the same approach for calculating the forcing of tropospheric ozone. Extensive tests were carried out to ensure that this approach yields sufficiently accurate forcing (S. Freidenreich, personal communication). Forcing is examined for two specific levels: top-of-the-atmosphere (TOA) and surface. Total-sky forcing takes into account the flux change occurring in the model's cloudless areas and in cloudy areas. In contrast, clear-sky forcing answers

Table 2a. Extinction Coefficients (σ_e) (m^2 g OC^{-1}), Single-Scattering Albedos (ω), and Asymmetry Factors (g) of Hydrophobic Organic Aerosol at 550 nm

	σ_e	ω	g
BASE	6.1	0.97	0.61
L-HYG	6.1	0.97	0.61
H-HYG	6.1	0.97	0.61
L-ABS	6.0	1.00	0.60
H-ABS	6.1	0.97	0.61

Table 2b. Same as Figure 1a, Except for Hydrophilic Organic Aerosol

	RH < 50%			RH = 80%			RH = 95%		
	σ_e	ω	g	σ_e	ω	g	σ_e	ω	g
BASE	5.4	0.97	0.61	7.9	0.98	0.66	18.8	0.99	0.74
L-HYG	5.4	0.97	0.61	5.4	0.97	0.61	5.4	0.97	0.61
H-HYG	5.4	0.97	0.61	10.3	0.98	0.69	28.8	0.99	0.77
L-ABS	5.3	1.00	0.60	7.9	1.00	0.66	18.8	1.00	0.74
H-ABS	5.4	0.97	0.61	8.0	0.96	0.66	18.9	0.96	0.74

what the forcing would be in the absence of clouds, thus avoiding interference caused by cloud fields on the calculated forcing, and providing a helpful mark for model intercomparison.

3. Results

3.1. Column Burdens

[15] The PI and PD mass column burdens of OC predicted with MOZART as driven by the same meteorological fields are plotted in Figure 2. In terms of sources, the naturally occurring biomass burning is primarily responsible for PI emissions. Relatively high burdens (1–2 mg m^{-2}) are found in some tropical and subtropical areas (i.e., Central Africa, South and East Asia) in January. In July, the part of South America that is covered by Amazonian forest claims some of the high burdens. The continents in the Northern Hemisphere (NH) such as eastern United States have peak organic aerosol burdens due to enhanced biomass burning during the summer time. The PI annual global mean burden of OC mass is 0.17 Tg OC.

[16] It is evident that anthropogenic burning of fossil fuels and biomass considerably elevates the atmospheric concentrations of organic aerosol. The emissions from the NH industrial areas, namely North America, Europe and East Asia, increase regional OC burdens approximately by 10 times relative to PI. As a result of long-range transport of organic aerosol, burdens over the oceans account for 50% of the global total. The PD annual global mean burden of OC mass reaches 1.36 Tg OC, much higher than the PI level of 0.17 Tg OC. The seasonal pattern of PD burdens is largely determined by that of OC emissions. The global mean PD burden in July is 40% higher than in January owing to increased fossil fuel and biomass burning. The layers near the surface contribute the most to column as the primary emissions are ground-based.

[17] Despite the large differences in burden, the PI and PD simulations yield similar geographical distributions in terms of the fraction of hydrophobic OC (Figure 3), which decreases as OC becomes increasingly hydrophilic during the process of being transported by winds horizontally as well as vertically. The fractions over the source regions are usually above 15%, and gradually decrease to around 5% over remote continental regions. OC burdens over oceans are almost entirely hydrophilic, except for the areas downwind of continental outflows that facilitate long-range

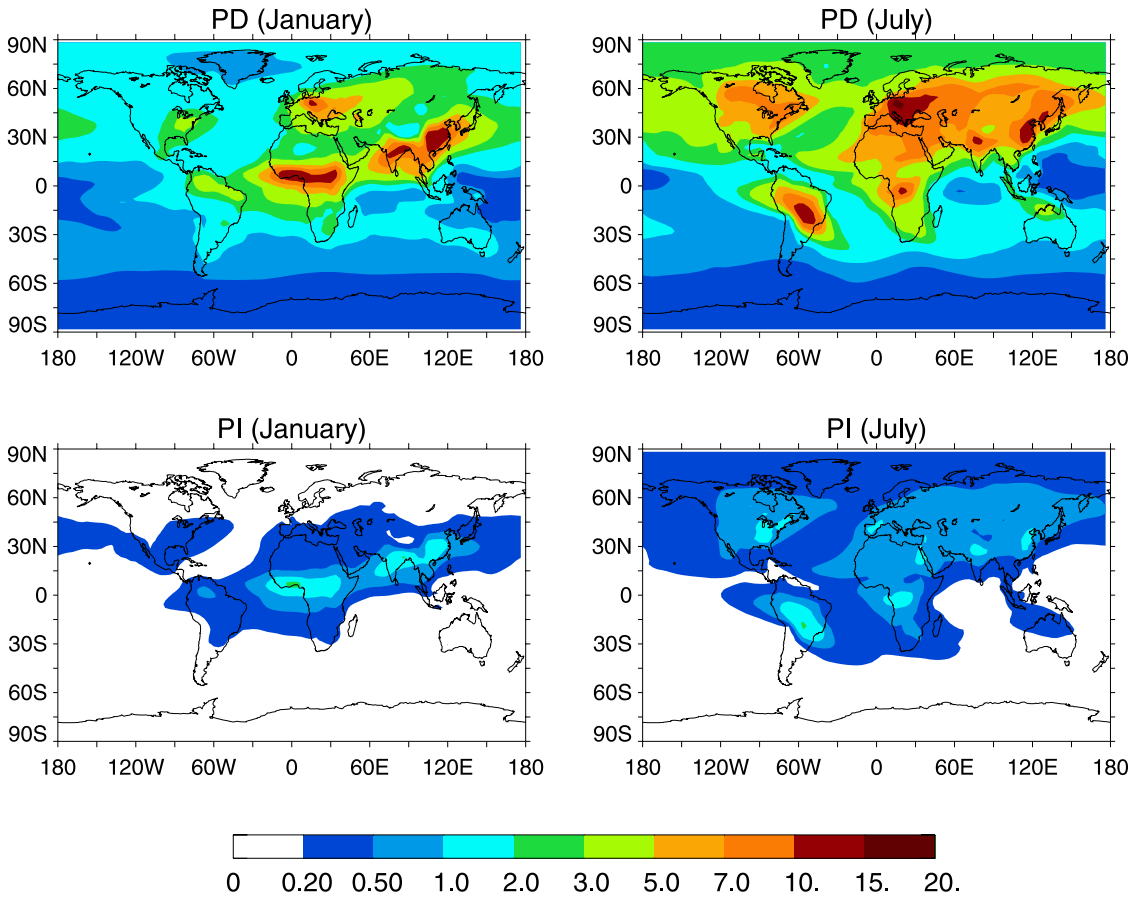

Figure 2. Column burdens (mg m^{-2}) of organic aerosol in January and July.

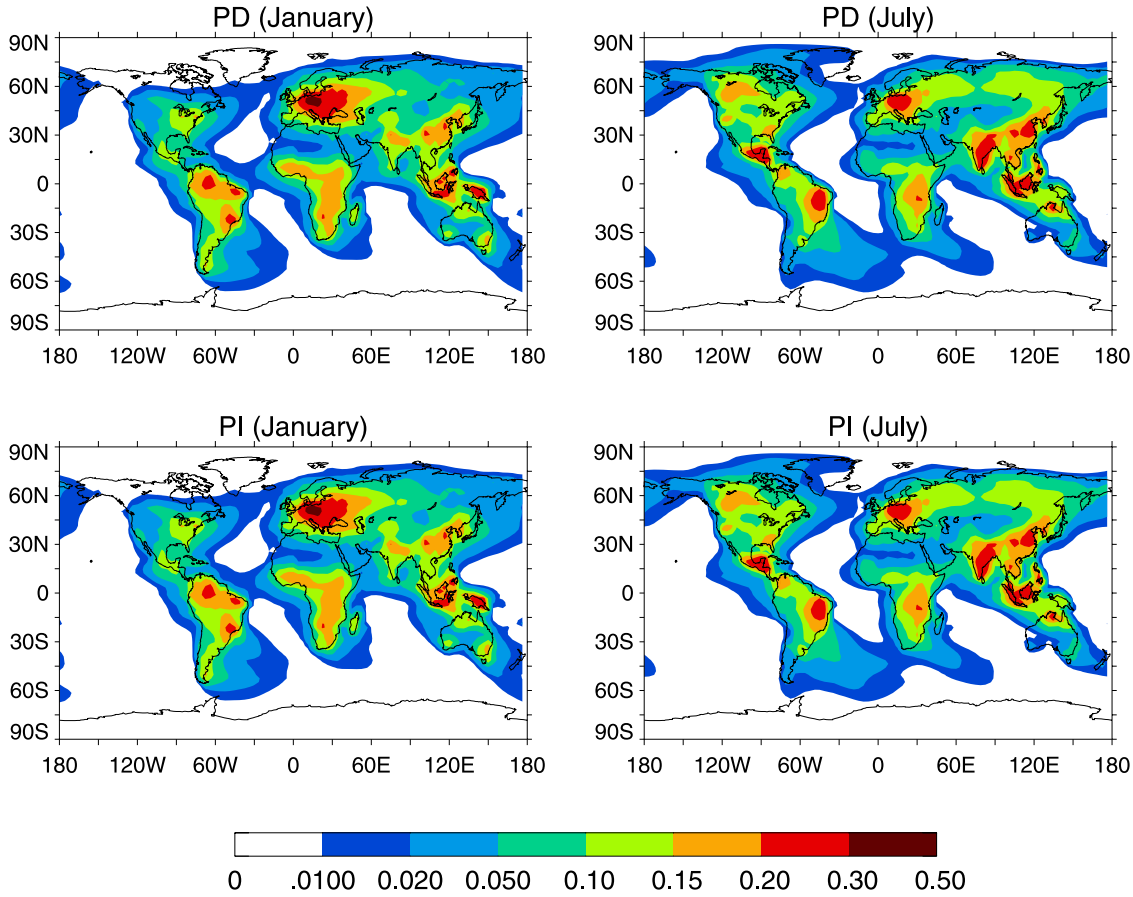

Figure 3. Fractions of hydrophobic organic aerosol in January and July.

transport of OC, and thus reduce the time available for atmospheric aging. The PD annual global mean burden of hydrophilic OC is 1.26 Tg OC, representing 93% of the total OC. The remaining OC burden of 0.10 Tg OC is hydrophobic. Since the OM/OC ratio is 1.3 for hydrophobic OC and 1.7 for hydrophilic OC, the average OM/OC ratio is calculated as 1.67.

3.2. Direct Radiative Forcing

[18] The particles resulting from anthropogenic sources increase backscattered and absorbed radiation. As shown in Figure 4, the total-sky TOA forcing of organic aerosol (solely in shortwave) is predominantly negative over the globe, exerting a net radiative cooling effect on the climate. The annual global mean amounts to -0.34 W m^{-2} (Table 3). The geographical distribution of forcing largely follows the pattern of burden. Due to the relatively high regional burdens, United States, Europe, East Asia, South America and Central Africa experience annual regional mean forcing as strong as -0.36, -0.75, -0.72, -0.67 and -0.89 W m^{-2}, respectively. In terms of the percentage of the total global forcing, these regions account for 2%, 4%, 5%, 6% and 8%, respectively. Overall the continents have a regional mean forcing of -0.46 W m^{-2}, representing only 41% of the total global forcing. Though this is seemingly low given that all OC emissions as well as highest burdens are located over land, it can be explained by two reasons. First, a large part of OC emissions is transported to oceans, which account for half of the total burden. Second, the residence time of the OC over oceans is longer than over land, rendering it more hygroscopic and thus more effective in scattering. The forcing over oceans generally lies in the range of 0 to -0.5 W m^{-2} with an annual mean of -0.28 W m^{-2} and claims the remaining 59% of the total forcing. Also plotted in Figure 4 is the total-sky surface forcing, which poses cooling across the globe with an annual mean of -0.63 W m^{-2}, almost all in shortwave. The surface forcing is considerably stronger than the TOA forcing due to absorption by organic aerosol in the atmosphere. Forcing as strong as -1 to -3 W m^{-2} is much more wide-spread at the surface than at TOA.

[19] An interesting feature is the mild warming over the Himalaya mountains and polar areas, all of which are characteristic of high surface albedo resulting from snow/ice cover. Because organic aerosol as modeled in this study is absorbing to some extent in visible wavelength, the upward shortwave radiation reflected by the surface is partially absorbed. This mechanism makes it possible for absorption to outweigh scattering, thereby registering a net warming.

[20] Under clear-sky conditions, those organic particles, which would otherwise be either underneath or in clouds, are exposed to incoming radiation. Thus the largely cooling effect of organic aerosol could be strengthened in the absence of clouds, a point that is affirmed by the clear-sky forcing plotted in Figure 5. The annual global mean

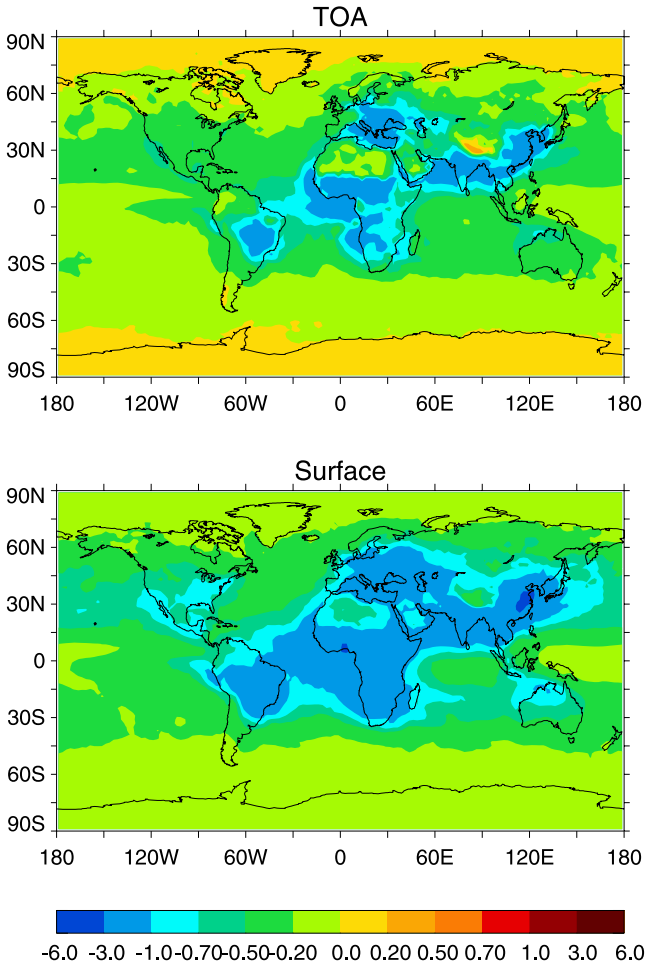

Figure 4. Annual mean total-sky TOA and surface forcing (W m^{-2}) of organic aerosol.

value of the clear-sky TOA forcing is −0.71 W m^{-2}, more than doubling the total-sky TOA forcing (−0.34 W m^{-2}). An examination of the geographical distribution reveals an even closer linkage between column burden and forcing than for the total-sky forcing. The clear-sky TOA forcing over the source regions as well as the oceanic regions downwind usually stays in the range of −1 to −3 W m^{-2}. The clearly-sky surface forcing is stronger, with an annual global mean of −0.98 W m^{-2}.

3.3. Seasonal Variations

[21] Like column burden, the calculated total-sky TOA forcing also undergoes strong seasonal variations. The monthly column burdens and forcings for some specific regions and the whole globe are plotted in Figure 6. It is interesting to note that even though the geographical distribution of forcing is largely determined by and subsequently is very similar to that of column burden, the temporal and spatial distribution of solar radiation also plays an important role in shaping seasonal variations. An example is that the forcing over Europe in January is not nearly as strong as the low-latitude Central Africa, while both areas have comparable aerosol burdens. On the global scale, the weakest total-sky TOA forcing of −0.25 W m^{-2} occurs in January, and the strongest of −0.46 W m^{-2} occurs in October, compared to the annual mean of −0.34 W m^{-2}.

Table 3. Annual Global Mean DRF[a]

	Total-Sky TOA Forcing	Clear-Sky TOA Forcing	Total-Sky Surface Forcing	Clear-Sky Surface Forcing
BASE	−0.34	−0.71	−0.63	−0.98
L-HYG	−0.28	−0.57	−0.58	−0.85
H-HYG	−0.40	−0.94	−0.69	−1.19
L-ABS	−0.50	−0.84	−0.49	−0.82
H-ABS	−0.26	−0.66	−0.67	−1.06

[a]Units are in W m^{-2}.

4. Sensitivity Analysis

4.1. Hygroscopic Growth

[22] There are two effects of hygroscopic growth on the optical properties of hygroscopic organic aerosol. First, increased liquid water makes wet particles more effective in extinction than dry ones. The extinction coefficient σ_e on the basis of per unit dry hydrophilic OC mass increases from 5.4 m^2 g^{-1} as dry to 18.8 m^2 g^{-1} at 95% RH in the BASE (standard) case (Table 2b). Second, since water is non-absorbing in visible wavelength, a wet particle has a smaller imaginary part of refractive index than a dry one,

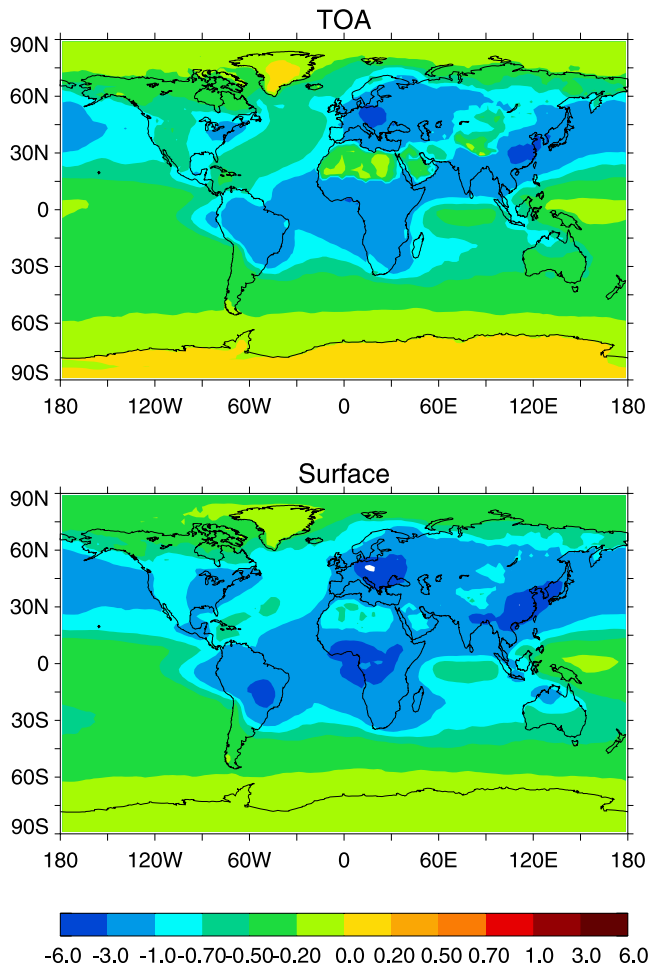

Figure 5. Annual mean clear-sky TOA and surface forcing (W m^{-2}) of organic aerosol.

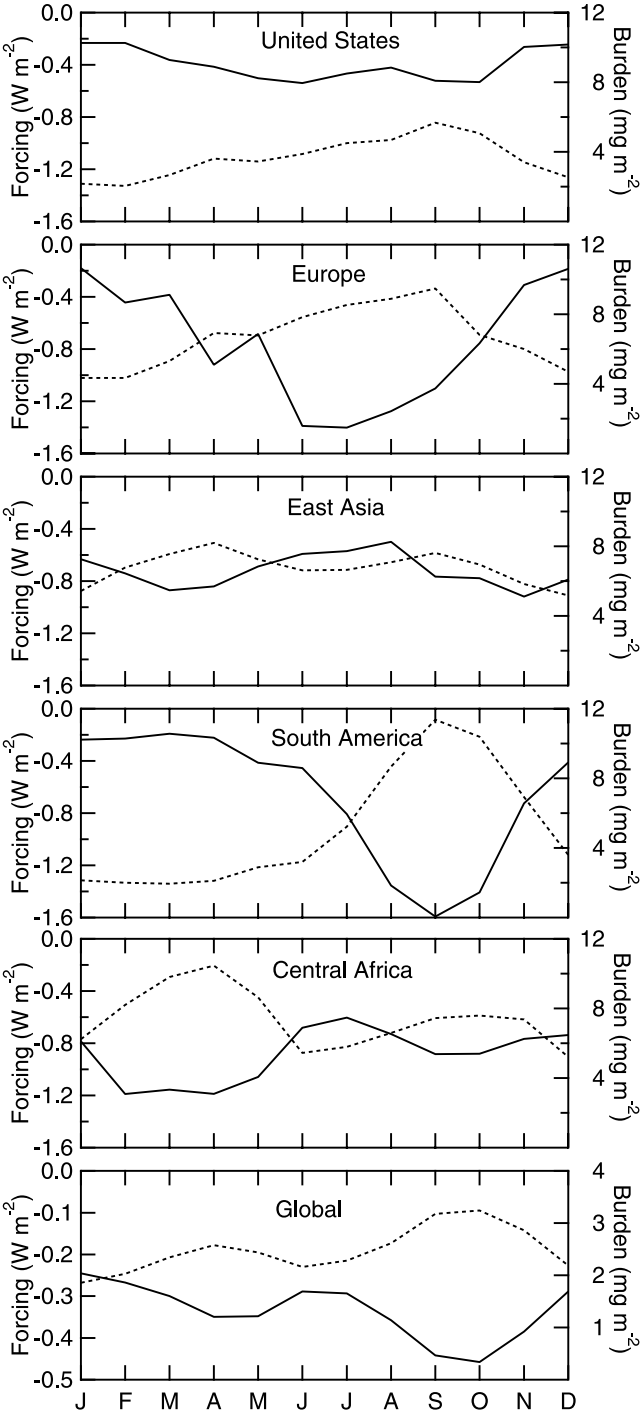

Figure 6. Seasonal variations of PD column burden (mg m^{-2}; dotted line) and total-sky TOA forcing (W m^{-2}; solid line) of organic aerosol.

thus becoming more effective in scattering. The single-scattering albedo ω increases from 0.97 for dry aerosol to 0.99 at 95% RH (Table 2b). In this sensitivity analysis, two limiting cases are employed to study the impacts of hygroscopic growth on different types of forcing.

[23] In the L-HYG (Low HYGroscopicity) case, hydrophilic OC is treated as non-hygroscopic, thus remaining in dry state regardless of ambient RH. As the lower bound of hygroscopicity, L-HYG keeps aerosol mass and the relevant optical properties invariant to RH (Table 2b). Note that L-HYG should be considered as a hypothetical case designed to underscore the importance of the property for the global forcing. Of course, atmospheric aging processes can eventually make particles hygroscopic to some extent [*Kanakidou et al.*, 2005]. However, this proves useful for quantifying the impacts on forcing due to neglect of hygroscopic growth. Malonic acid is a low-molecular-weight and highly soluble organic compound, and is generally more hygroscopic than the ones commonly found in the atmosphere (Figure 1). The H-HYG (High HYGroscopicity) case assumes that hydrophilic OC has the same hygroscopic growth factors as malonic acid, posing an upper bound on hygroscopicity. σ_e at 95% RH (28.8 m^2 g^{-1}) is 53% higher than in BASE (18.8 m^2 g^{-1}), which uses a model composition of four soluble compounds.

[24] As summarized in Table 3, the global annual mean values of total-sky TOA forcing in L-HYG and H-HYG are −0.28 and −0.40 W m^{-2}, respectively, compared to −0.34 W m^{-2} for BASE. Hygroscopic growth strengthens total-sky TOA forcing as a result of increased aerosol mass. The same effect can be seen more clearly in clear-sky TOA forcing, which is −0.57 W m^{-2} in L-HYG and −0.94 W m^{-2} in H-HYG, relative to −0.71 W m^{-2} in BASE. The total-sky and clear-sky surface forcing tabulated in Table 3 follow the same trend as their TOA counterparts as forcing is weakened in L-HYG, and strengthened in H-HYG. The percentage changes relative to BASE are approximately comparable to those in the TOA forcing. In terms of the difference between surface and TOA forcing, viz an evaluation of aerosol absorption in the atmosphere, the three cases show roughly equal amounts of absorption, though H-HYG is slightly less absorbing than the other two cases. This implies that the reduction in absorption caused by hygroscopic growth has negligible effect on the TOA forcing.

[25] The geographical distributions of the differences in total-sky TOA, total-sky surface, clear-sky TOA and clear-sky surface forcing between the sensitivity cases and BASE are plotted in Figures 7, 8, 9, and 10, respectively. Uniformly L-HYG is weaker and H-HYG is stronger than BASE for all types of forcing. The biggest differences generally occur over the source regions, where the highest burdens are located. The differences at TOA are similar to those at the surface both for total-sky and for clear-sky conditions. Under total-sky conditions, the reduced hygroscopic growth in L-HYG gives rise to a decrease of 0.2–0.5 W m^{-2} in cooling over the source regions, and 0–0.2 W m^{-2} elsewhere. H-HYG increases cooling by 0.2–0.5 W m^{-2} over the source regions, and by 0–0.2 W m^{-2} elsewhere. The absence of clouds (clear-sky) leads to larger differences, which amount to decreases as much as 0.5–3 W m^{-2} in L-HYG and increases of similar magnitudes in H-HYG over the source regions. Overall the continents account for 41% of the differences in total-sky TOA forcing both for L-HYG and for H-HYG.

4.2. Refractive Indices

[26] Though critical for determining optical properties, the refractive indices of organic aerosol assumed in BASE are subject to uncertainties due to the lack of measurements [*Kanakidou et al.*, 2005]. There is only one study on the

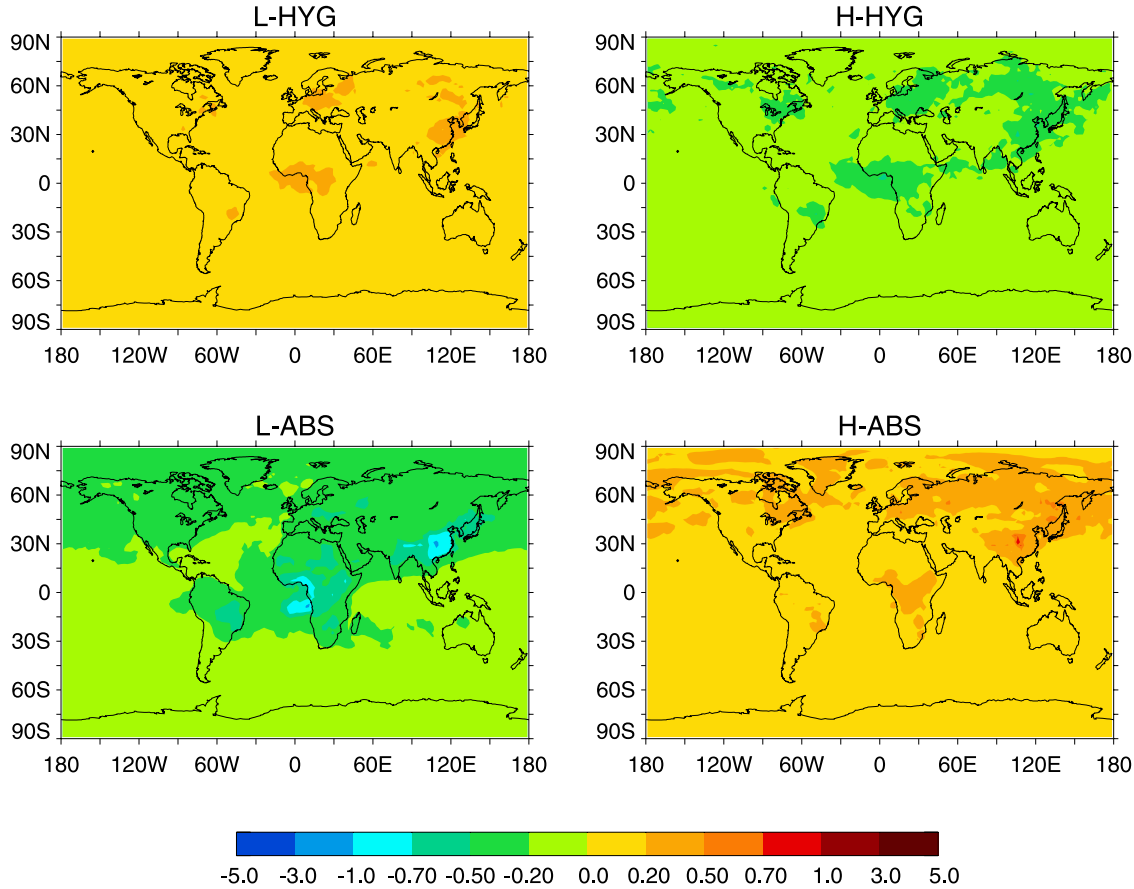

Figure 7. Differences in total-sky TOA forcing (W m^{-2}) between the sensitivity cases and BASE.

refractive indices of organic mixtures relevant to atmospheric aerosol. On the modeling side, most studies including *Cooke et al.* [1999], *Chung and Seinfeld* [2002], *Reddy et al.* [2005], and this one assume that OC is mildly absorbing in visible wavelength, and has the same refractive indices as the "water-soluble" aerosol defined in GADS. Thus we are unable to constrain refractive indices of OC either from measurements or from the range of values used in models. Instead, two hypothetical cases are used again to emphasize the significance of the property for the global forcing. The L-ABS (Low ABSorption) case treats organic aerosol the same as ammonium sulfate in terms of refractive indices. With an imaginary part as low as 10^{-7} in visible wavelength, organic aerosol is effectively non-absorbing (ω = 1.00; see Tables 2a and 2b). In the H-ABS (High ABSorption) case, instead of using volume averaging to account for water in a wet particle, the imaginary part of a wet particle is invariantly equal to that of a dry particle as assumed in BASE. Without taking into account the effect of non-absorbing water, wet particles as modeled in H-ABS are more absorbing than in BASE. ω of hydrophilic OC at a relatively high RH of 95% is 0.96 in H-ABS as opposed to 0.99 in BASE. Hygroscopic growth of particles in L-ABS and H-ABS is the same as in BASE.

[27] The annual global mean total-sky TOA forcing is -0.50 W m^{-2} in L-ABS and -0.26 W m^{-2} in H-ABS (Table 3). A comparison with BASE (-0.34 W m^{-2}) indicates that increased absorption reduces total-sky TOA forcing. For non-absorbing L-ABS, the surface forcing is very close to the TOA forcing. Under total-sky conditions, they are -0.50 and -0.49 W m^{-2}, respectively. In contrast, due to moderate absorption by organic aerosol in BASE and H-ABS, the surface forcing has the same sign as the TOA forcing (cooling), but is weaker than the TOA forcing. H-ABS, characteristic of the strongest absorption among the three cases, causes the biggest difference between the surface and total-sky TOA forcing (0.40 W m^{-2}).

[28] A comparison of Figures 7 and 8 shows that the variation in absorption gives rise to a reversal in the sign of forcing differences at TOA and surface. As organic aerosol becomes more absorbing, it reduces the outgoing radiation at TOA and the downward radiation at the surface, thus cooling down the surface and warming up TOA simultaneously. Relative to BASE, L-ABS strengthens TOA forcing by 0.5 to 1 W m^{-2} over the source regions, but reduces surface forcing to a similar degree. H-ABS does the opposite by decreasing TOA forcing and increasing surface forcing by 0.2 to 0.5 W m^{-2}. The differences in clear-sky forcing follow the same pattern, but are more pronounced. Overall the continents are responsible for 42% and 37% of the differences in total-sky TOA forcing for L-ABS and H-ABS, respectively.

5. Discussion

5.1. Sources of Uncertainties

[29] Numerous sources contribute to the uncertainties in the calculated DRF of organic aerosol and can be roughly

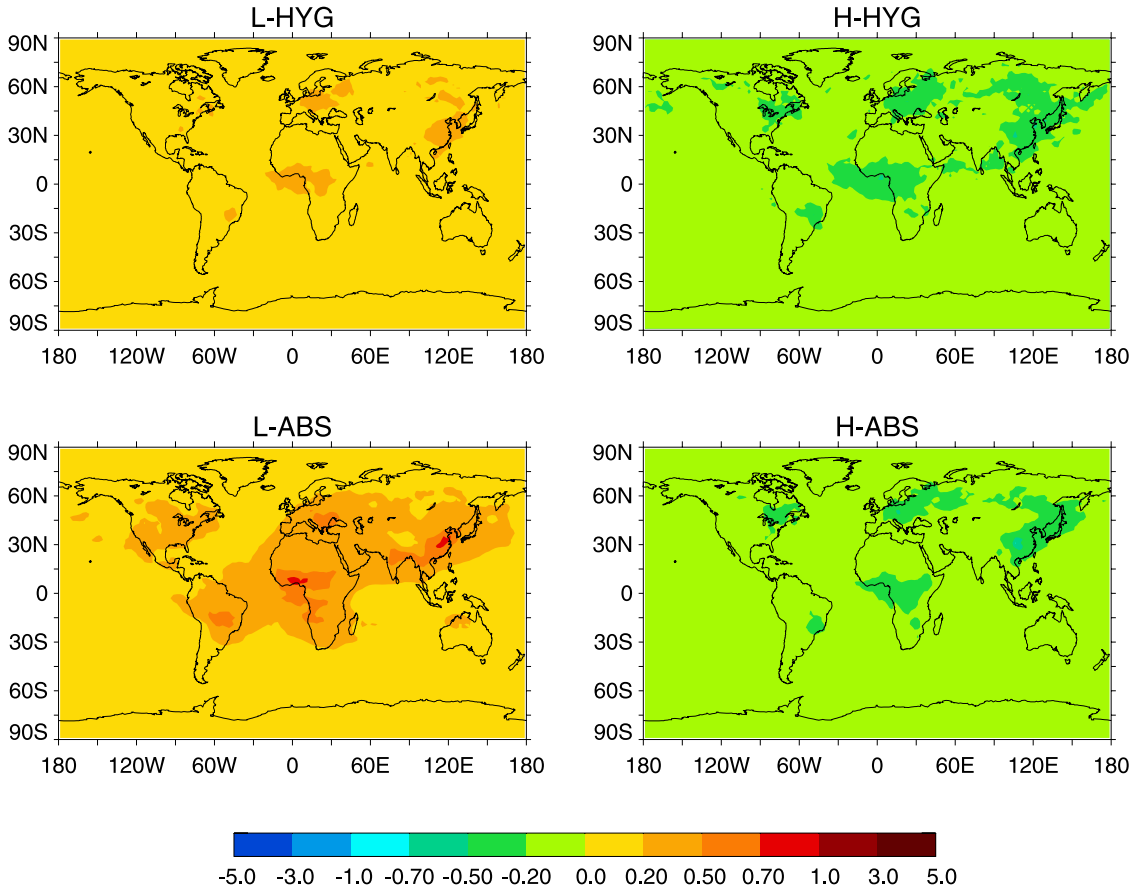

Figure 8. Differences in total-sky surface forcing (W m^{-2}) between the sensitivity cases and BASE.

classified into three categories. First, in order to simulate the temporal and spatial distribution of aerosol mass on the global scale, the current understanding of a series of processes from emissions to transport to chemical reactions to dry and wet deposition has to be improved. Second, aerosol mass is just one of the many parameters that determine the radiative properties of aerosol. The others include a set of fundamental physical and chemical properties (e.g., chemical composition, size distribution, solubility and mixing state). Third, technical issues related to the ability of GCMs to resolve environmental variables important for calculating aerosol forcing (e.g., RH and clouds) may add to uncertainties. Because the first type of sources of uncertainty is out of the scope of this paper, only the latter two will be discussed in further detail.

[30] Organic aerosol is treated as externally mixed with other aerosols such as sulfate and black carbon. However, both types of aerosol can be internally mixed either through co-emission or through microphysical processes like condensation and coagulation. As discussed by, e.g., *Chung and Seinfeld* [2002], the assumption of internal mixing gives rise to a reduction in total forcing compared to external mixing. *Ming and Russell* [2002] studied the impact of mixing state on hygroscopic growth, which, as well as its impact on refractive indices, should be included in future efforts to improve the representation of mixing state in forcing calculation.

[31] Hygroscopic growth of organic aerosol is very sensitive to RH, especially when it exceeds 80% (Figure 1). As GCMs track the amounts of water in different phases (i.e., vapor, liquid and ice), RH can be computed online in simulations and be used for calculating hygroscopic growth. However, as pointed out by *Adams et al.* [2001], the GCM–predicted RH has not been evaluated in a systematic fashion due to the lack of large-scale data. This work still remains to be done before more confidence can be put into RH and resulting forcing. It is also worth noting that as a result of the strong nonlinearity exhibited by hygroscopic growth factors to RH, using grid-average RH can potentially lead to an underestimation of water uptake and forcing [*Haywood et al.*, 1997].

[32] The cloud effect can be highlighted by comparing the ratio of clear-sky to total-sky TOA forcing, which is 2.2, 1.7 and 2.5 for BASE, L-ABS and H-ABS, respectively. Clearly the more absorbing organic aerosol is, the more susceptible total-sky forcing is to clouds and the vertical location of aerosol and clouds. This is because that DRF of absorbing organic aerosol is under impact of their location relative to clouds since those above can absorb the reflected or scattered solar radiation, thus reducing cooling. A similar finding has been made by *Haywood and Ramaswamy* [1998] for black carbon. Except for the change from cloud layer to surface, the same mechanism accounts for the net warming over the areas of high surface albedo shown in Figure 4. Therefore the accuracy of the calculated DRF at

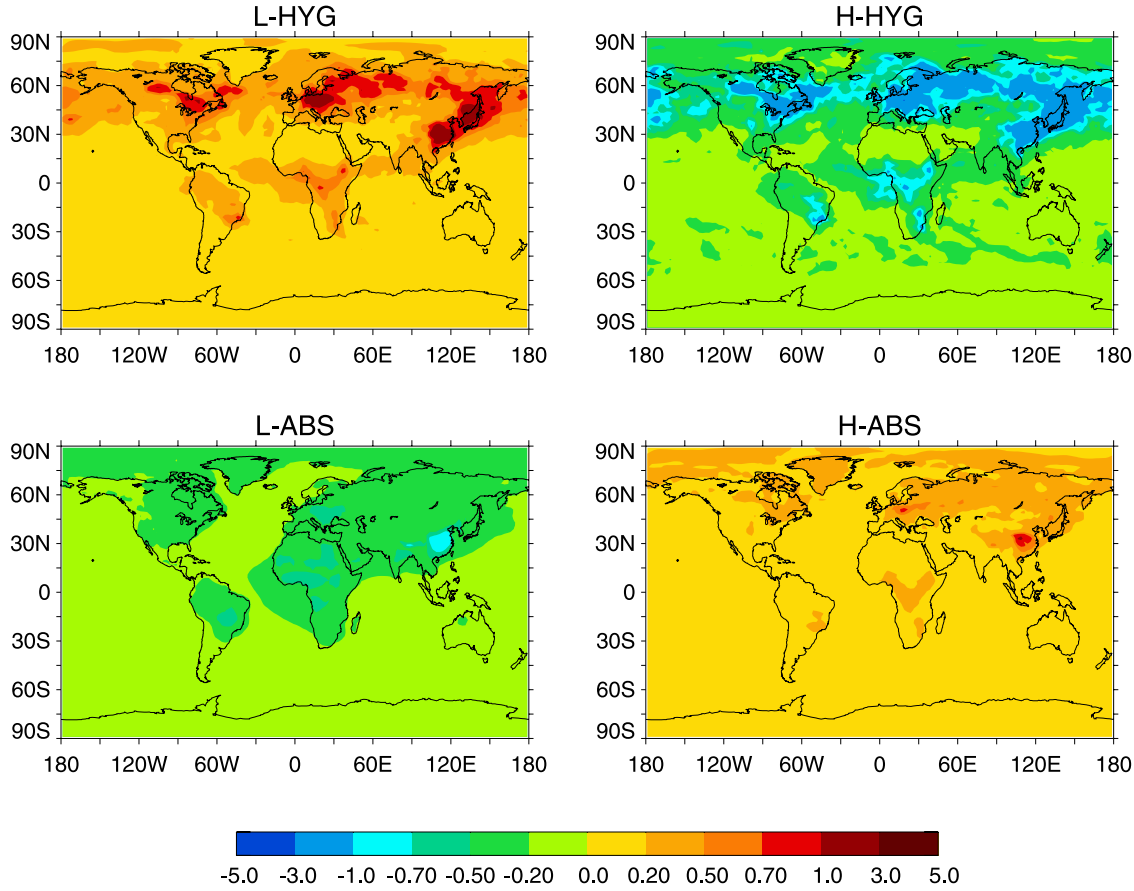

Figure 9. Differences in clear-sky TOA forcing (W m^{-2}) between the sensitivity cases and BASE.

least partially hinges on how well GCMs simulate both cloud amounts and vertical locations.

5.2. Comparison With Other Studies

[33] A few previous studies of the DRF of organic aerosol exist in the literature (Table 4). Some reported burdens of organic aerosol in terms of OM, which are converted to OC burdens using an average OM/OC ratio of 1.67. Most studies assumed that organic aerosol is externally mixed with other aerosols. The BASE (standard) case of this study yields a annual global mean total-sky TOA forcing of -0.34 W m^{-2} resulting from a global burden of 1.19 Tg OC. As a measure of forcing strength, the normalized forcing is formulated as the amount of forcing resulting from unit mass column burden of aerosol [see *Ramaswamy et al.*, 2001], and stands at -146 W g OC^{-1} for BASE. This removes, to the first order, the effect of different emissions used. *Cooke et al.* [1999] used the same extinction coefficient σ_e of 3.6 m^2 g OC^{-1} at 550 nm for hydrophobic and hydrophilic OC in dry state compared to 5.4 m^2 g OC^{-1} for hydrophilic OC and 6.1 m^2 g OC^{-1} for hydrophobic OC used in the study, owing to the differences in size distribution and density. The resulting normalized forcing of -70 W g OC^{-1} is significantly weaker than BASE (-146 W g OC^{-1}). For similar reasons, the extinction coefficient σ_e of 4.2 m^2 g OC^{-1} (2.5 m^2 g OM^{-1}) used in *Chung and Seinfeld* [2002] is smaller than those in this study. On the other hand, the hygroscopic growth of OC used in *Chung and Seinfeld* [2002] was modeled after inorganic salts, and is much stronger than in this study. Consequently, *Chung and Seinfeld* [2002] found that hygroscopic growth doubles forcing, in contrast to an increase of 55% in this study. These two compensating factors result in a normalized forcing of -98 m^2 g OC^{-1} compared to -146 W g OC^{-1} in BASE. *Koch* [2001] used a single extinction coefficient σ_e of 13.4 m^2 g OC^{-1} (8 m^2 g OM^{-1}) that is assumed to be applicable to an average RH. The average RH predicted by the GFDL GCM is around 80%, at which this study calculates σ_e at 7.9 m^2 g OC^{-1} for hydrophilic OC (Table 2b), considerably lower than that of *Koch* [2001]. This may explain why *Koch* [2001] reported an exceptionally high normalized forcing (269 W g OC^{-1}). The latest study of *Reddy et al.* [2005] assumed that organic aerosol has the same size distribution and hygroscopicity as sulfate, and reached an extinction coefficient σ_e of 5.3 m^2 g OC^{-1} (3.2 m^2 g OM^{-1}) in dry state, which is very close to 5.4 g OC^{-1} for hydrophilic OC in BASE. Even though the hygroscopicity of organic aerosol used in *Reddy et al.* [2005] is much stronger than in this study, they set an upper limit on RH at 95%. This treatment has an effect of reducing the effective hygroscopic growth, and results in a normalized forcing of -146 W g OC^{-1} that is the same as in BASE.

6. Conclusions

[34] This study simulates the DRF of organic aerosol using the GFDL GCM. The MOZART chemical transport

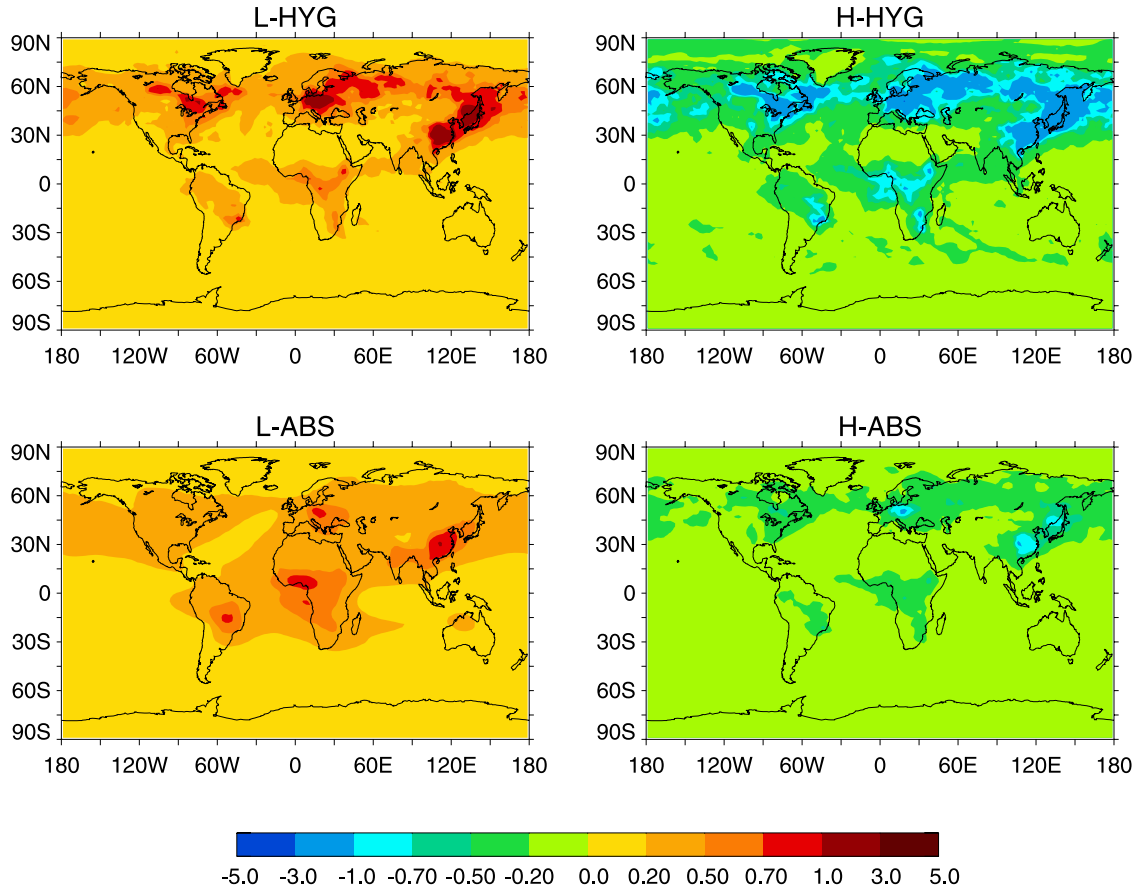

Figure 10. Differences in clear-sky surface forcing (W m^{-2}) between the sensitivity cases and BASE.

model provides the aerosol climatology. The PI and PD OC global burdens are 0.17 and 1.36 Tg OC, respectively. Differing from previous studies on the topic, the approach to calculating aerosol optical properties explicitly considers RH–dependent hygroscopic growth by employing a functional group–based thermodynamic model. Instead of assuming an arbitrary size distribution, this study makes use of the size distribution derived from AERONET measurements representative of biomass burning aerosol. Due to mild absorption in visible wavelength, the single-scattering albedo (ω) of hydrophobic OC in dry state is 0.97 and the extinction coefficient (σ_e) is 5.4 m^2 g OC^{-1} at 550 nm. Because of the increased scattering aerosol mass resulting from hygroscopic growth, σ_e is enhanced to 7.9 m^2 g OC^{-1} at 80% RH, and further to 18.8 m^2 g OC^{-1} at 95% RH.

[35] The annual global mean total-sky TOA and surface forcings are calculated to be −0.34 and −0.63 W m^{-2}, respectively, in the BASE case. Geographically the cooling largely lies over the source regions, namely part of South America, Central Africa, Europe and South and East Asia, though the areas of high surface albedo experience mild warming resulting from enhanced absorption. The annual global mean clear-sky TOA and surface forcings are −0.71 and −0.98 W m^{-2}, respectively.

[36] The sensitivity analyses show that hygroscopic growth enhances considerably the negative forcing. Complete deprivation of water uptake reduces the total-sky TOA forcing by 18%, while the uptake by malonic acid, a highly soluble organic compound, enhances the forcing by 18%. The total-sky TOA forcing is also sensitive to the absorption

Table 4. Comparison of OC Burden, DRF, and Normalized Forcing With Other Studies

	Hygroscopic (Yes/No)	Absorbing (Yes/No)	Burden, Tg OC	DRF, W m^{-2}	Normalized Forcing, W g OC^{-1}
This study	Yes	Yes	1.19	−0.34	−146
This study	No	Yes	1.19	−0.25	−120
This study	Yes	No	1.19	−0.48	−215
Cooke et al. [1999][a]	Yes	Yes	0.17	−0.024	−70
Koch [2001][b,c]	Yes	Yes	0.57	−0.30	−269
Chung and Seinfeld [2002][c]	Yes	Yes	0.89	−0.18	−98
Chung and Seinfeld [2002][c]	No	Yes	0.89	−0.09	−49
Reddy et al. [2005][c]	Yes	Yes	1.05	−0.30	−146

[a]Only fossil fuel sources.
[b]Hygroscopic growth is fixed at a certain relative humidity.
[c]The burden of OM was reported, and converted to OC using a OM/OC ratio of 1.67.

properties of organic aerosol. Treating them as non-absorbing increases the forcing by 47%, while neglecting the scattering by condensed water causes a reduction of 24%. A question to be pursued in future studies is the significance of the range in forcing emerging from the sensitivity studies here relative to other sources of uncertainties, such as meteorology and long-range transport of organic aerosol.

References

Adams, P. J., J. H. Seinfeld, D. Koch, L. Mickley, and D. Jacob (2001), General circulation model assessment of direct radiative forcing by the sulfate-nitrate-ammonium-water inorganic aerosol system, *J. Geophys. Res.*, *106*, 1097–1111.

Andreae, M. O., and P. Merlet (2001), Emission of trace gases and aerosols from biomass burning, *Global Biogeochem. Cycles*, *15*, 955–966.

Chung, C. H., and J. H. Seinfeld (2002), Global distribution and climate forcing of carbonaceous aerosols, *J. Geophys. Res.*, *107*(D19), 4407, doi:10.1029/2001JD001397.

Cooke, W. F., C. Liousse, H. Cachier, and J. Feichter (1999), Construction of a $1^\circ \times 1^\circ$ fossil fuel emission data set for carbonaceous aerosol and implementation and radiative impact in the ECHAM4 model, *J. Geophys. Res.*, *104*, 22,137–22,162.

Dubovik, O., B. Holben, T. F. Eck, A. Smirnov, Y. J. Kaufman, M. D. King, D. Tanre, and I. Slutsker (2002), Variability of absorption and optical properties of key aerosol types observed in worldwide locations, *J. Atmos. Sci.*, *59*, 590–608.

Duce, R. A., V. A. Mohnen, P. R. Zimmerman, D. Grosjean, W. Cautreels, R. Chatfield, R. Jaenicke, J. A. Ogren, E. D. Pellizzari, and G. T. Wallace (1983), Organic material in the global troposhpere, *Rev. Geophys.*, *21*, 921–952.

GFDL Global Atmospheric Model Development Team (2004), The new GFDL global atmosphere and land model AM2-LM2: Evaluation with prescribed SST simulations, *J. Clim.*, *17*, 4641–4673.

Hao, W. M., and M. H. Liu (1994), Spatial and temporal distribution of tropical biomass burning, *Global Biogeochem. Cycles*, *8*, 495–503.

Haywood, J. M., and V. Ramaswamy (1998), Global sensitivity studies of the direct radiative forcing due to anthropogenic sulfate and black carbon aerosols, *J. Geophys. Res.*, *103*, 6043–6058.

Haywood, J. M., V. Ramaswamy, and L. J. Donner (1997), A limited-area-model case study of the effects of sub-grid scale variations in relative humidity and cloud upon the direct radiative forcing of sulfate aerosol, *Geophys. Res. Lett.*, *24*, 143–146.

Haywood, J. M., M. D. Schwarzkopf, and V. Ramaswamy (1998), Estimates of radiative forcing due to modeled increases in tropospheric ozone, *J. Geophys. Res.*, *103*, 16,999–17,007.

Horowitz, L. W., et al. (2003), A global simulation of tropospheric ozone and related tracers: Description and evaluation of MOZART, version 2, *J. Geophys. Res.*, *108*(D24), 4784, doi:10.1029/2002JD002853.

Kanakidou, M., et al. (2005), Organic aerosol and global climate modelling, a review, *Atmos. Chem. Phys. Discuss.*, *4*, 5855–6024.

Koch, D. (2001), Transport and direct radiative forcing of carbonaceous and sulfate aerosols in the GISS GCM, *J. Geophys. Res.*, *106*, 20,311–20,332.

Köpek, P., M. Hess, I. Schult, and E. P. Shettle (1997), Global aerosol data set, *Tech. Rep. 243*, Max Planck Inst., Hamburg, Germany.

Liao, H., J. H. Seinfeld, P. J. Adams, and L. J. Mickley (2004), Global radiative forcing of coupled tropospheric ozone and aerosols in a unified general circulation model, *J. Geophys. Res.*, *109*, D16207, doi:10.1029/2003JD004456.

Liousse, C., J. E. Penner, C. Chuang, J. J. Walton, H. Eddleman, and H. Cachier (1996), A global three-dimensional model study of carbonaceous aerosols, *J. Geophys. Res.*, *101*, 19,411–19,432.

Middlebrook, A. M., D. M. Murphy, and D. S. Thomson (1998), Observations of organic material in individual marine particles at Cape Grim during the First Aerosol Characterization Experiment (ACE 1), *J. Geophys. Res.*, *103*, 16,475–16,483.

Ming, Y., and L. M. Russell (2001), Predicted hygroscopic growth of sea salt aerosol, *J. Geophys. Res.*, *106*, 28,259–28,274.

Ming, Y., and L. M. Russell (2002), Thermodynamic equilibrium of organic-electrolyte mixtures in aerosol particles, *AIChE J.*, *48*, 1331–1348.

Mueller, J.-F. (1992), Geographical distribution and seasonal variation of surface emissions and deposition velocities of atmospheric trace gases, *J. Geophys. Res.*, *97*, 3787–3804.

Prenni, A. J., P. J. DeMott, S. M. Kreidenweis, D. E. Sherman, L. M. Russell, and Y. Ming (2001), The effects of low molecular weight dicarboxylic acids on cloud formation, *J. Phys. Chem.*, *105*, 11,240–11,248.

Ramaswamy, V., et al. (2001), Radiative forcing of climate change, in Climate Change 2001: The Scientific Basis, Contribution of Working Group I to the Third Assessment Report of the Intergovernmental Panel on Climate Change (IPCC), edited by J. T. Houghton et al., pp. 349–416, Cambridge Univ. Press, New York.

Randles, C. A., L. M. Russell, and V. Ramaswamy (2004), Hygroscopic and optical properties of organic sea salt aerosol and consequences for climate forcing, *Geophys. Res. Lett.*, *31*, L16108, doi:10.1029/2004GL020628.

Reddy, M. S., O. Boucher, Y. Balkanski, and M. Schulz (2005), Aerosol optical depths and direct radiative perturbations by species and source type, *Geophys. Res. Lett.*, *32*, L12803, doi:10.1029/2004GL021743.

Rogge, W. F., M. A. Mazurek, L. M. Hildemann, G. R. Cass, and B. R. T. Simoneit (1993), Quantification of urban organic aerosol at a molecular–level – Identification, abundance and seasonal–variation, *Atmos. Environ., Part A*, *27*, 1309–1330.

Russell, L. M. (2003), Aerosol organic-mass-to-organic-carbon ratio measurements, *Environ. Sci. Technol.*, *37*, 2982–2987.

Tie, X., G. Brasseur, L. Emmons, L. Horowitz, and D. Kinnison (2001), Effects of aerosols on tropospheric oxidants: A global model study, *J. Geophys. Res.*, *106*, 22,931–22,964.

Tie, X., S. Madronich, S. Walters, D. P. Edwards, P. Ginoux, N. Mahowald, R. Zhang, C. Lou, and G. Brasseur (2005), Assessment of the global impact of aerosols on tropospheric oxidants, *J. Geophys. Res.*, *110*, D03204, doi:10.1029/2004JD005359.

Turpin, B. J., and H.-J. Lim (2001), Species contribution to PM2.5 mass concentrations: Revisiting common assumptions for estimating organic mass, *Aerosol Sci. Technol.*, *35*, 602–610.

P. A. Ginoux, L. H. Horowitz, and V. Ramaswamy, Geophysical Fluid Dynamics Laboratory, Princeton, NJ 08542, USA. (paul.ginoux@noaa.gov; larry.horowitz@noaa.gov; v.ramaswamy@noaa.gov)

Y. Ming, Visiting Scientist Program, University Corporation for Atmospheric Research, Geophysical Fluid Dynamics Laboratory, Princeton, NJ 08542, USA. (yi.ming@noaa.gov)